AGU PUBLICATIONS

JGR

Journal of Geophysical Research: Solid Earth

RESEARCH ARTICLE
10.1002/2014JB011657

Key Points:
- Conductivity structure imaged under a basin covered with extensive magmatism
- Quasi-linear conductive zones served as feeder conduits for basaltic extrusion
- Crust beneath the central part of the basin impregnated by conducting minerals

Supporting Information:
- Figures S1–S6

Correspondence to:
A. L. Padilha,
antonio.padilha@inpe.br

Citation:
Padilha, A. L., Í. Vitorello, C. E. Antunes, and M. B. Pádua (2015), Imaging three-dimensional crustal conductivity structures reflecting continental flood basalt effects hidden beneath thick intracratonic sedimentary basin, *J. Geophys. Res. Solid Earth*, *120*, 4702–4719, doi:10.1002/2014JB011657.

Received 30 SEP 2014
Accepted 23 JUN 2015
Accepted article online 25 JUN 2015
Published online 14 JUL 2015

Imaging three-dimensional crustal conductivity structures reflecting continental flood basalt effects hidden beneath thick intracratonic sedimentary basin

Antonio L. Padilha[1], Ícaro Vitorello[1], Cassio E. Antunes[1], and Marcelo B. Pádua[1]

[1]Instituto Nacional de Pesquisas Espaciais, São José dos Campos, Brazil

Abstract A large-scale array of long-period magnetic data and a deep-probing magnetotelluric profile were recorded in the intracratonic Paraná sedimentary basin in central eastern South America, which presents a thick and extensive sedimentary-magmatic sequence that allows its basement to be investigated only by indirect methods. Integration of the results from both methods showed that the crust beneath the basin presents several quasi-linear highly conductive channeled zones with limited lateral extent, in coincidence with some of the main tectonic structures recognized at the surface, and a moderate but pervasive lithosphere conductivity enhancement beneath its central part. Upward movement of CO^2-bearing volatiles and magmas precipitating highly conducting mineral phases along discrete subvertical fault zones that served as feeder conduits for Early Cretaceous voluminous continental flood basalts was a likely process responsible for the localized conductivity enhancements. Correlation between some of the linear conductive zones and elongated magnetic anomalies and between the maximum depth occurrence of most of these conductive anomalies and the Curie depth at which crustal rocks lose their magnetism gives strong support to interconnected iron oxides (especially magnetite) and iron sulfides (such as pyrrhotite) as the main conductive sources. The moderate bulk conductivity increase in the crust and upper mantle beneath the central part of the basin is unexpected for a postulated cratonic basement and is tentatively associated with impregnation of the lithosphere by conducting minerals related either to widespread tectonic events in the Ordovician or Late Precambrian or to dispersed magmatic residues of an Early Cretaceous magma differentiation contaminating the entire lithosphere.

1. Introduction

Intracratonic basins are recognized by their large dish-shaped extensions and are distinguished from extension or compression basins that are originated from clearly related tensional processes. On the contrary, intracratonic basins have their mechanisms of origin and evolution not yet well understood, although there are a large number of evolutionary models often invoked in the literature. These include the cooling of a mechanically stretched continental lithosphere, cooling related to sublithospheric mantle flow, densification of the underlying lithosphere due to deep phase changes, surface response to magmatism and/or plume activity, and long-wavelength buckling under in-plane stresses (see review by *Allen and Armitage* [2012]). Apart from the possible complexity of the processes responsible for the origin and evolution of these basins, the lack of corroborative geophysical data certainly contributes to this large range of interpretative alternatives.

A very wide segment of the central eastern South America lithospheric plate is covered by intraplate basins which have relatively less geophysical information than the extensional basins of the Brazilian continental margin or the foreland sub-Andean basins. Among the South American intracratonic basins, the Paraná Basin is one that has the largest collection of geological, geochemical, and geophysical data. The importance of the geophysical studies in the Paraná Basin arises because much of the sedimentary layers and basement is only accessible by methods of indirect investigations or very deep boreholes, due to its thick sedimentary-magmatic sequence (thickness up to 7000 m at its depocenter) [*Zalán et al.,* 1990]. Thus, the present-day knowledge about the structural framework of the basin has been achieved primarily from sparse and shallow drillings of the sedimentary package [e.g., *Cordani et al.,* 1984] and few geophysical surveys, particularly seismic reflection [*Marques et al.,* 1993], potential methods [*Ferreira*, 1982; *Molina et al.,* 1988],

very limited magnetotellurics [*Stanley et al.,* 1985; *Padilha et al.,* 1992] and more recent receptor function [*Julià et al.,* 2008], seismic tomography [*Rocha et al.,* 2011], and satellite studies [*Mariani et al.,* 2013].

One of the main results from these studies has been the suggestion of some important regional tectonic structures beneath the basin, which has held differing interpretations regarding its tectonosedimentary evolution. The subsidence mechanisms that have been proposed for the Paraná Basin include its development over a zone of mechanical weakness in the upper crust associated with the breakup of a Late Precambrian supercontinent, which acted as a focusing heat lens that caused partial melting of the lower crust and subsequent intrusion of anorogenic granites during extensional tectonics [*Klein and Hsui*, 1987], subsidence due to the lithospheric cooling of the region after the Neoproterozoic Brasiliano Orogeny [*Zalán et al.,* 1990], or in response to rifting and transtensional reactivation of mechanically weak zones in the Late Ordovician, followed by regional flexure in the Devonian [*Milani and Ramos*, 1998]. Similarly, the configuration of the crystalline basement of the basin is disputed, with propositions of a single cratonic block under the basin axial region surrounded by Brasiliano mobile belts [*Cordani et al.,* 1984; *Mantovani et al.,* 2005] or a collage of several cratonic blocks separated by a number of interposed suture zones [*Milani and Ramos*, 1998].

The lower crust and upper mantle beneath the Paraná Basin are still much less known, especially along the western and southern portions of the basin. In fact, the seismic stations used until now in deep tomographic mappings are mainly concentrated north of latitude 25°S [*Rocha et al.,* 2011], generating interpretative limitations when comparing these data with those from geoid anomalies [*Molina and Ussami*, 1999], which also provide complementary information on the deeper parts of the lithosphere. Because of this, there are many unknown aspects of the geodynamical response of the continental lithosphere to the large tectonomagmatic events that occurred in the basin between the Proterozoic and Cenozoic.

Large-scale electromagnetic (EM) induction soundings are largely used to provide images of the electrical conductivity structure of the crust and mantle lithosphere [*Selway*, 2014]. The spatial resolution of these EM induction methods is commonly less than other imaging methods, such as seismology, because EM methods exploit diffusive energy propagation instead of wave energy propagation. However, EM methods compensate for its limitations in resolution with its sensitivity to changes in electrical conductivity, a parameter that varies by many orders of magnitude within the Earth materials [*Evans*, 2012]. Such a large variation in conductivity ensures a higher resolution, particularly laterally, compared to other geophysical methods. Moreover, variation in electrical conductivity is related to minor constituents of rocks, thus providing unique geological information complementary to the bulk properties of rocks given by other deep-sounding geophysical methods.

Deep EM induction studies have proven to be effective in mapping lithospheric structures beneath sedimentary basins, as shown, for instance, in studies of the intracratonic Parnaíba Basin in north northeast Brazil [*Arora et al.,* 1998, 1999]. In our paper, we analyze transient geomagnetic variations recorded by an array of 63 stations around the central part of the Paraná Basin to infer the three-dimensional (3-D) electrical conductivity structure beneath this part of the basin. Geomagnetic depth sounding (GDS) responses, related to the ratio of vertical magnetic field (H_z) to the horizontal fields (H_x and H_y), are used to map geological structures marked by large lateral conductivity contrasts. Limited depth resolution of the GDS method is overcome by using constraints from a two-dimensional (2-D) magnetotelluric survey and geoid results. Well-defined conductivity patterns are identified beneath the basin and interpreted as reflecting paleochannels in the basement that probably favored the upward flow of various Early Cretaceous magmatic events.

2. Geological Setting

The intracratonic Paraná Basin is a major Phanerozoic feature in central eastern South America, having an irregular oval shape with the major axis in the NNE direction. The basin comprises a thick and extensive sedimentary-magmatic sequence, which covers an approximate area of 1,700,000 km^2, mainly in southern Brazil but also in Uruguay, Paraguay, and Argentina. A generalized geological map of the Brazilian part of the basin is shown in Figure 1.

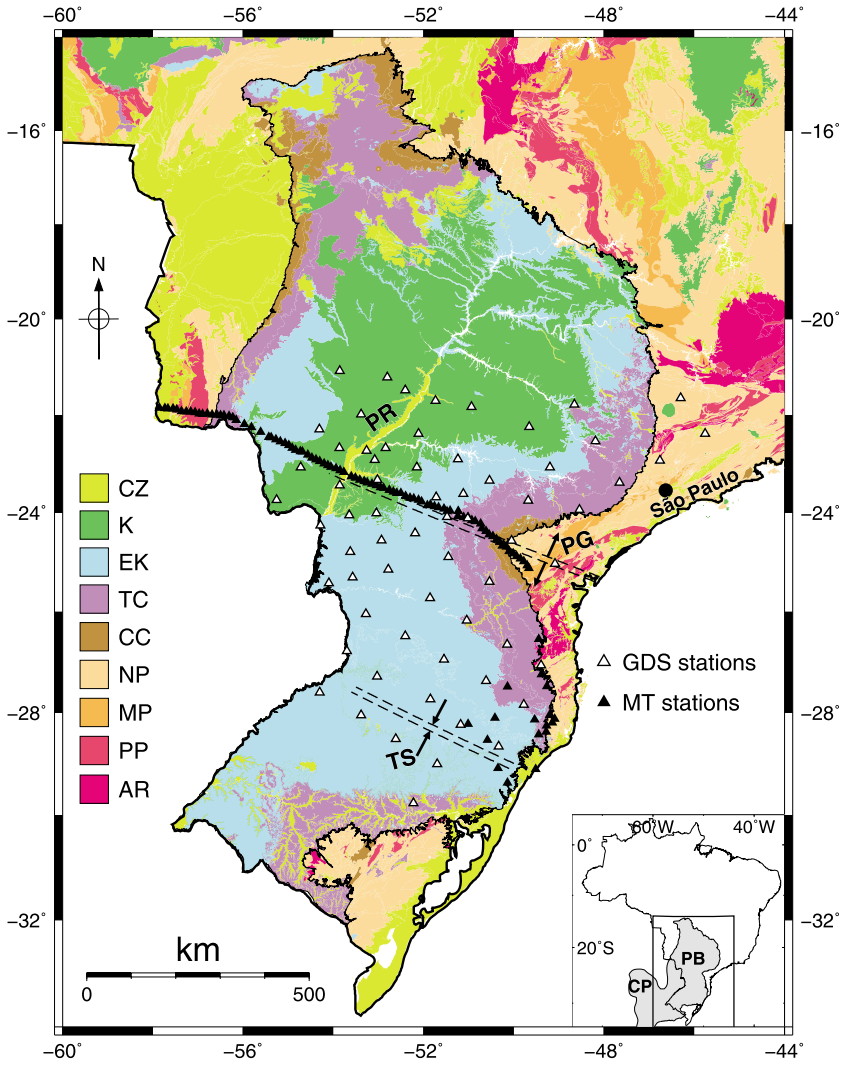

Figure 1. Generalized geological map of southern Brazil, with emphasis on the Brazilian part of the Paraná Basin (geology from *Bizzi et al.* [2001]). Locations of magnetic and magnetotelluric stations are shown as open and closed triangles, respectively. Main structures are the following: PR = Paraná River; PG = Ponta Grossa Arch; and TS = Torres Syncline and its WNW extension composing the Torres-Posadas lineament. Geological periods of outcrops are the following: CZ = Cenozoic; K = Cretaceous sediments; EK = Early Cretaceous basalts; TC = Triassic-Carboniferous; CC = Carboniferous-Cambrian; NP = Neoproterozoic; MP = Mesoproterozoic; PP = Paleoproterozoic; and AR = Archean. Inset shows the study area with the full areal extent of the Paraná Basin (PB) and contiguous Chaco-Paraná Basin (CP).

The limits of the Paraná Basin are delineated by syntectonic and posttectonic activity of arches and structural lineaments, parallel or transverse to its borders. Geological mapping, aeromagnetic and gravity data, and a few scattered stratigraphic wells define that the major structural trends affecting the basin are in NW and NE directions. The NW trending is associated with fault zones hosting a swarm of diabase dikes, whereas fault zones without the emplacement of dikes characterize the NE trending elements [*Zalán et al.,* 1990]. Subordinated E-W trending structures are also described by *Zalán et al.* [1990]. Notable are the NW structures, nearly parallel to several arches, the Torres Syncline, and various tectonic and/or magnetic lineaments. All these tectonic structures evolved since the Devonian and were particularly active in Triassic to Jurassic periods [*Fúlfaro et al.,* 1982].

The basin stratigraphic succession encompassing Late Ordovician to Late Cretaceous sequences summarizes a long, polycyclic evolutionary history, corresponding to at least three transgressive-regressive cycles strongly influenced by glaciation, sea level changes, and intraplate stresses derived from Andean orogenies

[*Zalán et al.,* 1990; *Milani and Ramos*, 1998]. The sedimentary sequence of predominantly siliciclastic and carbonate rocks started deposition during the Late Ordovician. The first stage of subsidence (Ordovician to Silurian and Devonian) includes mainly continental sandstones and marine rocks that were deposited in a gulf environment opened toward the Panthalassa Ocean. The NW tectonics was particularly active, and a general uplift related to Andean Eo-Hercynian orogenesis caused the interruption of the sedimentation during Late Devonian-Mississippian. The second phase of subsidence (Permo-Carboniferous) corresponds to a voluminous package of sedimentary rocks in which the sedimentation evolved from glacial to fluvio-deltaic environments and finally to marine conditions. The NW and NE tectonics were alternatively active during this period, and a general uplift interrupted sedimentation in the Late Permian-Early Triassic causing the sea to no longer reach the basin. The sedimentation recommenced during the Middle Triassic, when eolian sandstone beds began to dominate, causing subaerial sedimentation and increasing aridity, with the development of large sand dune systems. An important control on the Triassic-Jurassic sedimentation was provided by the NW and E-W tectonics.

In the Early Cretaceous, just prior to the breakup of the Gondwana supercontinent in the South Atlantic region, the Paraná Basin was inundated by extensive lava flows and emplacement of abundant dikes and sill-type intrusions, composed mostly of tholeiitic basalts with minor rhyolites and rhyodacites in the upper portion [*Melfi et al.,* 1988]. This volcanism covers an area of about 1,200,000 km^2 and comprises 780,000 km^3 of extrusive material, with a maximum thickness of approximately 1700 m. From gravity and isostatic evidences, it has been proposed that part of the magmatic material was not extruded and resides as a magmatic underplating at the lower crust [*Molina et al.,* 1988; *Mariani et al.,* 2013]. According to *Janasi et al.* [2011], the entire magmatism occurred in only 3 Ma (~134.5–131.5 Ma), extruding first along NE trending faults in the central part of the basin and further migrating to the southeast along the NW striking lineaments that constitute the Ponta Grossa Arch at about the same time that coast-parallel dikes formed near the southeastern Brazilian onshore coastal margin. Alkaline and alkaline-carbonatitic complexes are also found mainly along the present-day rim of the basin in close association with the tholeiitic flood basalts and dike swarms, ranging in age from Early Cretaceous to Paleocene [*Gomes and Comin-Chiaramonti*, 2005]. Geochemically, the basalts are divided into two groups on the basis of Ti contents: the southern part is characterized by dominantly low-Ti content and the northern part by high-Ti content [*Bellieni et al.,* 1984]. *Rocha-Júnior et al.* [2012] propose that the northern high-Ti basalts were derived from a sublithospheric mantle enriched by fluids and/or magmas associated with Neoproterozoic subduction processes. There are controversies about the processes involved in the basalt genesis with propositions that its composition substantially reflects a deep asthenospheric mantle plume (Tristan da Cunha) source [*Gibson et al.,* 1995] or an alternative nonplume-related model with the magmatism triggered by a large thermal anomaly at the coast of West Africa [*Ernesto et al.,* 2002]. After the basaltic volcanism, in the Late Cretaceous, the northern part of the basin subsided and a thin layer of continental sediments was deposited ending the depositional history of the basin.

3. GDS Study

The GDS method is related to the relationship between horizontal (H_x and H_y) and vertical (H_z) magnetic field components

$$H_z = T_{zx}H_x + T_{zy}H_y, \tag{1}$$

where T_{zx} and T_{zy} denote the complex vertical geomagnetic transfer functions (VTF). They are often represented as complex induction arrows,

$$T_z = T_{zx}\hat{x} + T_{zy}\hat{y}, \tag{2}$$

where $\hat{x}$ and $\hat{y}$ are unitary vectors. These arrows are a graphical representation of the VTF projected onto a plain (normally a map of station locations). Following the convention of *Parkinson* [1959], the real arrows are reversed to point toward regions of high conductivity and away from resistive blocks.

Transient geomagnetic variations were recorded with three-component fluxgate magnetometers [*Chamalaun and Walker*, 1982] in several array deployments between 2002 and 2006, yielding a total of 212 sites in central and southern Brazil [*Bologna et al.,* 2014]. At each array deployment, the magnetic fields were recorded over periods of at least 6 weeks using a 60 s sampling interval, with at least one station common to

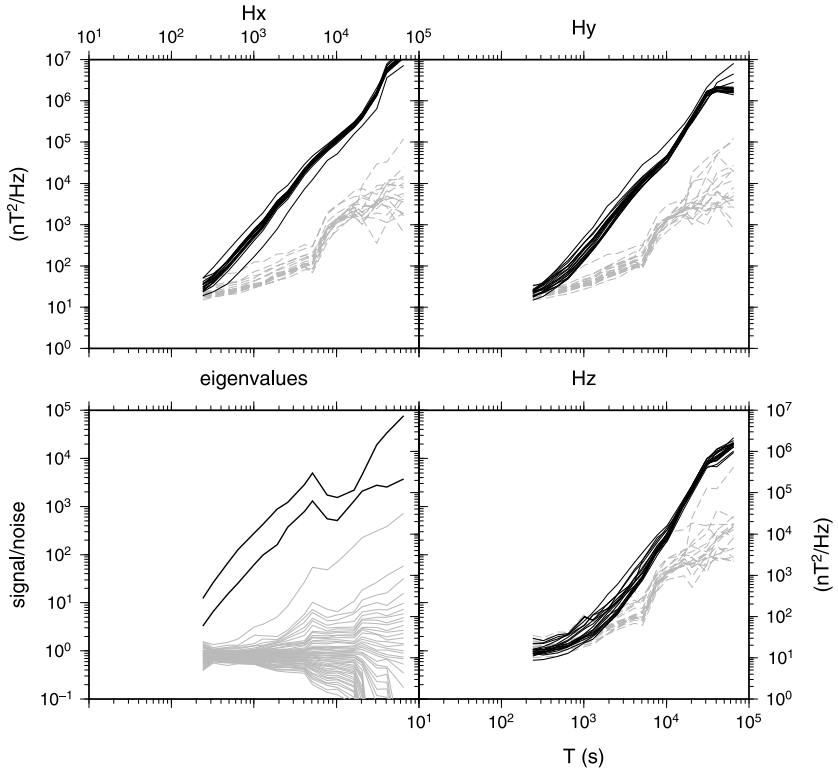

Figure 2. Multivariate analysis of the spectral density matrix (SDM) from data of 17 stations in one of our GDS subarrays. Shown are the estimated signal spectra (black solid lines) and incoherent noise spectra (gray dashed lines) computed for the three magnetic channels and the eigenvalues of the scaled SDM (obtained by the division of the estimated incoherent noise standard deviations) interpreted as signal-to-noise power ratios. The two dominant eigenvalues used to compute the vertical transfer functions are plotted as solid lines.

two adjoining arrays being used as reference for calculation of the VTF. Details about general magnetometer operation, data acquisition, and reduction steps are given in *Rigoti et al.* [1999] and *Antunes* [2012]. Part of these data has been selected to infer the configuration of internal induced currents beneath the central part of the Paraná Basin. The geological map in Figure 1 shows the location of the 63 geomagnetic stations chosen for this study.

3.1. Data Processing

The recorded time series from each subarray were processed using the robust processing scheme of *Egbert* [1997] based on multivariate statistical methods. When applied to array data, this procedure provides a powerful tool for estimating the VTF by removing incoherent noise and identifying coherent noise, either due to cultural noise or spatial complexity of the natural sources [*Egbert*, 2002]. An example of multivariate analysis of the spectral density matrix (SDM) for data in one of our subarrays is shown in Figure 2. SDM is a matrix of averaged cross products for all components observed in the 17 sites operated simultaneously in this specific array. Estimated signal and incoherent noise power spectra in the three magnetic channels of all stations as well as the eigenvalue spectra are plotted as a function of period.

Incoherent noise is significant for the shortest periods, where signal-to-noise ratios for the fluxgate magnetometers are small, and at some specific sites, especially in the vertical component. The approach taken in sites with evidence of noise was to check the time series, remove sections possibly contaminated with noise, and repeat the process. In cases where there was no improvement after several attempts, the contaminated sites were discarded from further analysis. For this subarray, only one site was discarded because of severe incoherent noise.

Also, over a wide period range, the two largest eigenvalues exceed significantly the others, corresponding roughly to two polarizations of uniform magnetic sources. This means that the array data are consistent

with plane wave sources with no coherent noise [*Egbert and Booker*, 1989]. However, at periods longer than 2000 s, a third significant eigenvalue is clearly observed, indicating the presence of coherent noise and/or source effects on the data. This general pattern is seen in all our overlapping subarrays and also in a previous geomagnetic array study carried out at nearly the same latitude in western South America [*Soyer and Brasse*, 2001]. The large area covered by these surveys and the period range affected suggest that the noise cannot be generated by an artificial source of coherent noise. Also, associating this long-period effect to a small number of data samples [*Soyer and Brasse*, 2001] does not hold for our data. More properly, one additional independent source is probably required to characterize the spatially coherent observations.

Further analysis and processing would be required to allow a quantitative interpretation of this third eigenvalue [e.g., *Egbert*, 2002], which are beyond the scope of this paper. Notwithstanding this caveat, a potential connection with effects generated by the South Atlantic magnetic anomaly (SAMA) can be presumed. The SAMA covers most of South America and is characterized by the lowest values of the geomagnetic field intensity at the Earth's surface associated with either the eccentricity of the geomagnetic dipole axis [*Fraser-Smith*, 1987] or reverse magnetic fluxes in the Earth's outer core under this region [*Hulot et al.,* 2002]. As a consequence, azimuthally drifting energetic particles trapped in the Earth's inner Van Allen radiation belt come closest to the Earth's surface, by that interacting with the dense atmosphere and producing enhanced ionization at ionospheric *E* layer heights (see *Paulikas* [1975] for a review). This extra ionization-producing enhanced ionospheric conductivity is a regular feature of the ionosphere over the SAMA even under magnetically quiet conditions that can be further enhanced during magnetically disturbed periods [*Abdu et al.,* 2005]. Large-scale spatial gradients in conductivity arising from this particle precipitation process can generate localized electric field structure within the SAMA thus producing systematic effects on the VTF estimates due to the finite spatial scale of the source. Alternatively, the plane wave approximation used to derive the VTF can be violated at midlatitude in periods longer than 10,000 s due to contamination from the solar quiet daily (Sq) variation and its higher harmonics [*Shimizu et al.,* 2011].

In the simplest approach, it is assumed that the two eigenvectors associated with the two largest eigenvalues correspond to two polarizations of the plane wave source fields and are used to compute the VTF [*Egbert and Booker*, 1989]. However, as shown in Figure 2, in our data set nonhomogeneous effects can be significant at periods longer than 2000 s. To quantify the impacts of possible violations of the uniform source approximation at these periods, we used a heuristic approach. Assuming that the VTF must be smooth and representing an acceptable distribution of conductivity within the Earth, a preliminary 3-D inversion of the VTF data in the period range between 300 and 20,000 s was performed. A parallelized version of the ModEM code of *Egbert and Kelbert* [2012] was used for inverting the data of all 63 stations at seven periods within the above referred period range. Figure 3 shows a comparison between the measured and predicted data presented in terms of real and imaginary VTF for the 16 selected sites of the subarray of Figure 2. In general, the experimental data are smooth functions of period and present good fit with the predicted model data, suggesting statistically stable and reliable estimates. However, at periods longer than 10,000 s, the VTF at all sites increases dramatically in amplitude, not fitting the model data. These very sharp jumps in the real and imaginary parts of the VTF are purely due to the source geometry so that no information about the Earth structure can be obtained. To avoid external source bias on our results, periods longer than 10,000 s were discarded.

3.2. Induction Arrows

A qualitative recognition of lateral conductivity contrasts in the subsurface can be inferred by plotting the induction arrows. Figure 4 displays maps of the real induction arrows for four periods together with a schematic outline of the Paraná Basin in southern Brazil, where small periods are more sensitive to shallow and local structures and longer periods to deep and regional structures. The arrows are plotted in the Parkinson convention and point toward regions with higher conductivity. Their lengths are a function of the conductivity contrast and also decrease with distance from the conductor.

At the shortest period (480 s) the arrows have a complex pattern responding to shallower conductivity contrasts close to the sites. Although the station spacing is not sufficiently dense to delineate finer-scale patterns in detail, there are several reversals in the direction of the arrows between neighboring sites, a diagnostic of localized conductive structure underneath these regions. The most important of these

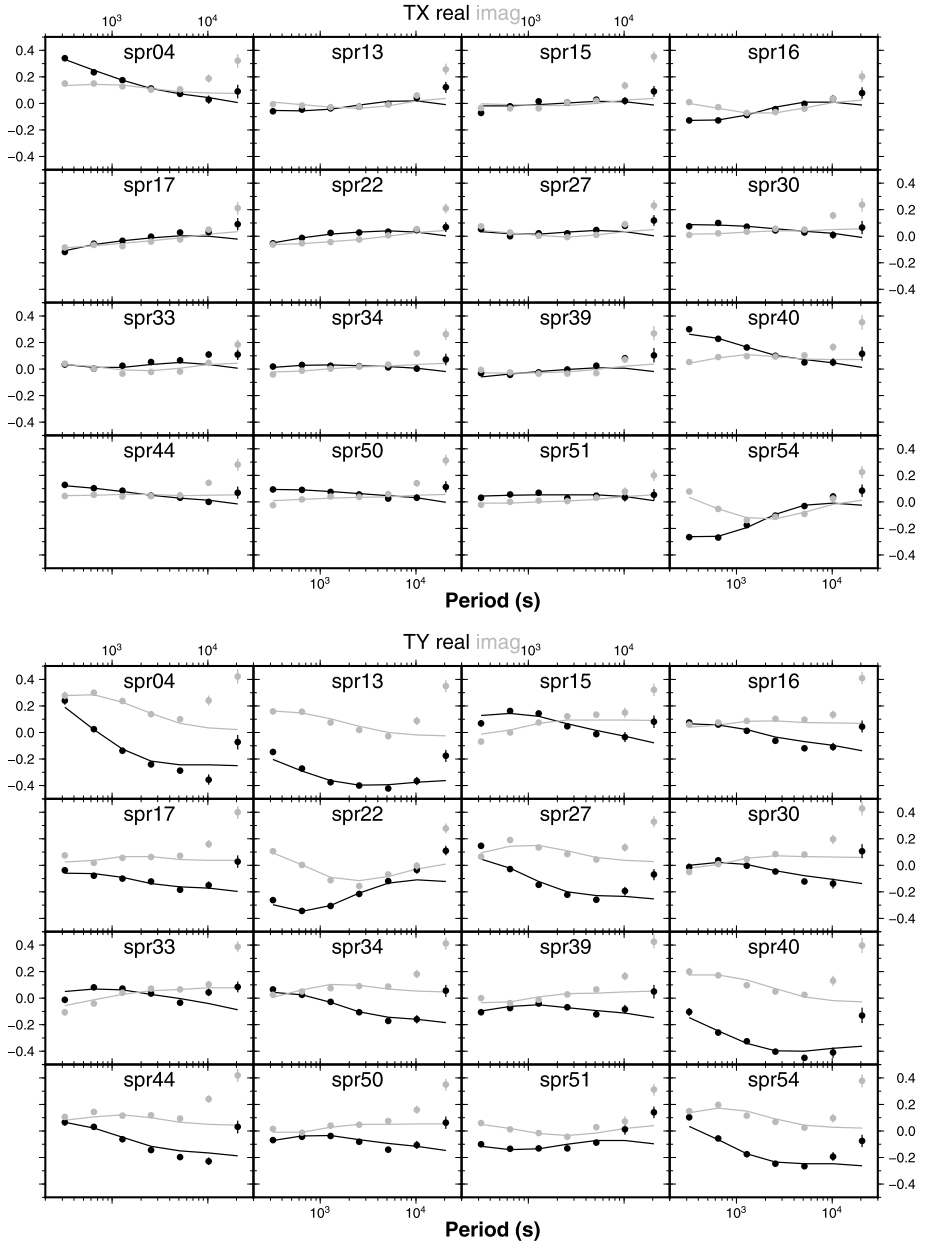

Figure 3. Comparison between measured (dots) and predicted (solid lines) vertical transfer functions derived from a preliminary 3-D inversion model. Real transfer functions are in black and imaginary transfer functions in gray for 16 sites of the subarray shown in Figure 2.

structures is located close to the basin depocenter and seems to characterize an elongated conductive feature running approximately NNE. It is roughly parallel to the Paraná River (see Figure 1) and closely follows the trend of maximum thicknesses of sediments and basalts [*Zalán et al.,* 1990].

A similar pattern persists at 1020 s, but beyond 2580 s the inductive picture undergoes a systematic change, with the arrows on the eastern side of the array swinging to a direction roughly perpendicular to the nearest coastline and the arrows on the central part of the basin decreasing significantly in magnitude. The former, the oceanward effect, is related to the sharp contrast in conductivity between the relatively more resistive land and the more conductive ocean at shallow depths which will produce an electric current concentration in the conducting seawater flowing parallel to the coastline [*Parkinson and Jones*, 1979]. The latter, the decreasing magnitude effect, indicates that no significant lateral conductivity variation occurs at the subsurface below

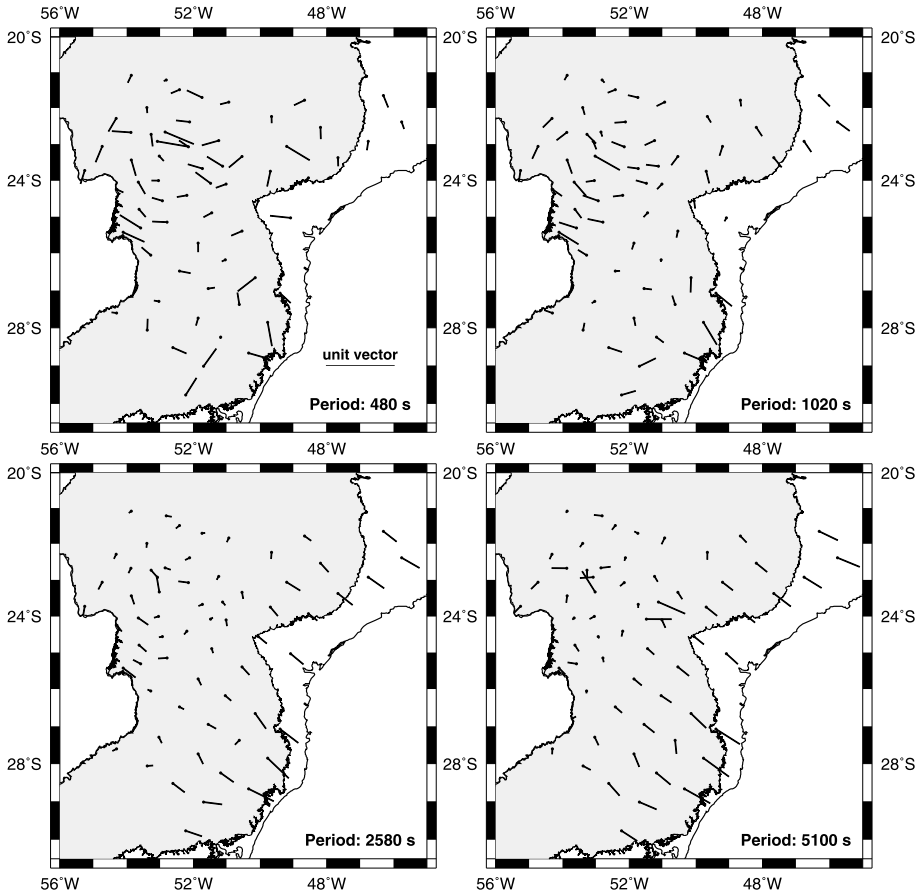

Figure 4. Real induction arrows of four periods shown in a map with a schematic outline of the Paraná Basin in southern Brazil. Arrows have been reversed to point toward induced internal currents.

(one-dimensional structure) or that the measurements were carried out just above the center of a regional conducting feature beneath the central part of the basin.

At the longest period (5100 s), the responses are smoothed and spatially expanded, due to the averaging effect of increased penetration depth, and show the primary electrical conductivity structure directly. The pattern is simple and summarized in effects of the eastern coastline (now influencing induction arrows located at a distance of several hundred kilometers from the coast) and near null arrows to the west of the array. It can be noted that the anomalous effects of the current concentration along the central part of the basin are still observed at the longest period.

4. Inversion Models

The analysis of the induction arrows showed the presence of large and complex conducting structures beneath the Paraná Basin. A 3-D geoelectrical model of the south central region of the basin was generated through 3-D inversion of the VTF data. The ModEM code [*Egbert and Kelbert*, 2012] was used to fit the VTF responses at seven selected periods logarithmically spaced between 300 and 10,000 s, with a constant absolute error set at 0.02. The coordinate system was chosen to be approximately parallel to the shoreline, and accordingly, the horizontal grid was rotated 30° from north to east. The 3-D model was discretized to be regular in the area of interest, with horizontal cell widths of 10 km. The mesh comprised a total of 190 cells in the *x* direction (NW), 162 cells in the *y* direction, and 58 cells in the vertical. The thickness of the 12 top layers was 500 m, and the thickness of each subsequent layer increased with a vertical factor of 1.15. For all inversions discussed in the following sections, the same model smoothing (model covariance parameters) value of 0.3 was applied in all directions and the Atlantic Ocean (0.3 Ω m

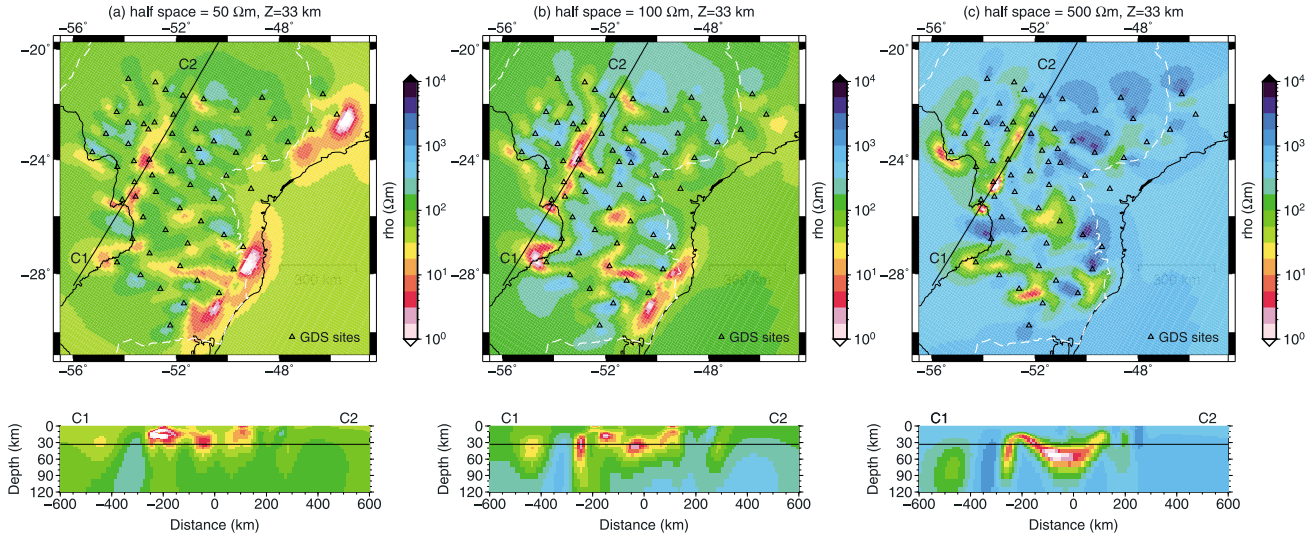

Figure 5. Three-dimensional inversion results as derived from three different half-space starting models. Figures 5a–5c (top) show horizontal resistivity maps at a depth of 33 km inverted from half-spaces of (a) 50 Ω m, (b) 100 Ω m, and (c) 500 Ω m, superimposed on the outline of the Paraná Basin (dashed white lines) in southern Brazil and with the location of the GDS sites. Figures 5a–5c (bottom) show vertical resistivity sections of the model immediately above, along the profile C1-C2.

seawater resistivity) was included as a priori structure using known bathymetry and kept fixed during the inversion procedure.

4.1. Preliminary 3-D Inversion Tests

Multiple inversion runs were conducted with several starting models, including layered-Earth models and different resistivity half-space models, to assess resolution of model features. In the following discussion, we will focus on the inversion starting from homogeneous half-space models with different resistivities to show the inherently nonunique model resulting when using the VTF data alone.

Three-dimensional inversion results derived from three different starting models are summarized in Figure 5. Perspective views at a lower crustal (33 km) depth and vertical cross sections along a profile nearly parallel to the Paraná River are shown for inversions from 50, 100, and 500 Ω m half-space prior models, which resulted in root-mean-square misfits (RMS) between observations and model predictions of 2.08, 1.80, and 1.93, respectively. Detailed analysis of the RMS distribution between sites for the different models has shown that there are no large areas where the 3-D inversion models are systematically unable to explain the data (areas with large RMS).

Generally, the resistivity distribution is similar in the different models with high-conductivity anomalies being detected at nearly the same locations. The conductive anomalies located external to the array near the coastline and clearly seen in the two more conductive models are also observed in the resistive model (500 Ω m half-space) but at greater depths. The same is observed when comparing the other anomalies in the models, which are detected in approximately the same horizontal location but at different vertical positions and with different amplitudes. This result is not unexpected since previous tests with synthetic examples have shown that inversion of VTF data alone can only recover the horizontal position and lateral conductivity contrasts of anomalous structures, but not their depths and absolute values of resistivity [e.g., *Siripunvaraporn and Egbert*, 2009]. These same tests have also shown that a starting model close to the correct host resistivity improves recovering the correct resistivity structure with inversion of VTF data alone. This constraint on background resistivities can be provided by an inversion of magnetotelluric (MT) measurements.

4.2. Two-Dimensional Magnetotelluric Constraints

Figure 1 shows the location of a 950 km long WNW-ESE MT profile across the central part of the Paraná Basin. The MT method uses simultaneous measurements of natural time variations in the horizontal and vertical components of the magnetic field and the corresponding changes in the horizontal components of the induced electric field to obtain lateral and vertical conductivity variations in the interior of the Earth.

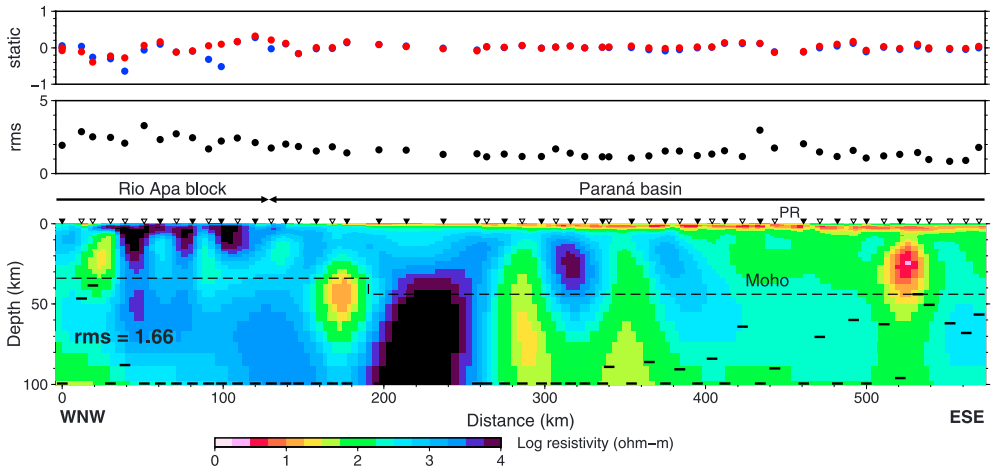

Figure 6. (top) The estimated static shift coefficients in units of log of apparent resistivity (red for TE mode and blue for TM mode) and (middle) the RMS errors of individual stations. (bottom) The 2-D resistivity model of the central western part of the profile across the Paraná Basin from inversion of magnetotelluric data, with indication of the surficial limits of the geological domains. MT sites are represented by open triangles for broadband-only soundings and closed triangles for the joint broadband and long-period soundings. PR stands for the position of the Paraná River. Moho depth (black linear dashes) is estimated mainly from receiver function analyses [*Assumpção et al.,* 2013], and short horizontal bars represent the estimated maximum depth of investigation beneath each site, following the procedure described by *Padilha et al.* [2013]. Bars plotted at the 100 km level have even deeper penetration.

Five-component MT data were recorded at 92 sites along the profile that was deployed parallel to the Ponta Grossa Arch in the eastern border of the basin and cuts nearly perpendicularly the C1-C2 traverse of Figure 5.

The recorded time series were processed using the robust code of *Egbert* [1997] to estimate the complex MT transfer functions relating the measured EM fields. Reliable response function estimates were obtained for the entire period range at most sites in the western and central parts of the profile, but a significant decrease in data quality was observed in the eastern part of the profile. This is likely associated with a ±600 kV high-voltage direct current transmission line crossing obliquely the profile at 51°W longitude and contaminating MT responses of 19 sites. These sites, as well as the 11 uncontaminated sites located at the eastern end of the profile, were discarded from further analysis.

Tensor decomposition analysis was used on data from the central and western parts of the profile to define the dimensionality of the data, derive a regional 2-D geoelectric strike direction, and remove effects of galvanic scatters [*Groom and Bailey*, 1989]. The remaining unknown static shift related to near-surface inhomogeneities causing a shift in the log apparent resistivity was determined as part of the inversion procedure. Except for some sites over the outcropping resistive rocks of the Rio Apa block on the western end of the profile, acceptable fits to the measured data were observed in the decomposition analysis. The overall strike is aligned in the NNE direction, but the eight easternmost sites present strike angles mostly in the NNW direction. These sites were excluded, and a multisite, multiperiod analysis [*McNeice and Jones*, 2001] on the remaining 54 sites gives acceptable fits to the measured impedance data for a regional strike of N14°E, roughly coincident with the main direction of the conductivity anomaly parallel to the Paraná River and the direction of the profile C1-C2, shown in Figure 5. Accordingly, distortion models were fit to the data with the N14°E strike direction, with the electrical current flowing along the strike direction defining the TE mode while the perpendicular responses defined the TM mode.

The 2-D inversion of the decomposed data was conducted using the REBOCC code [*Siripunvaraporn and Egbert*, 2000], fitting both the TE and TM modes simultaneously. The data were initially inverted for the TM mode alone to account for off-profile structures. To minimize static shift effects, phase fitting was also emphasized by using larger error floor in the apparent resistivities. The resulting model was used as the starting model for the joint inversion of the TM and TE data, with error floors successively reduced. The final inversion was run with error floors of 10% in apparent resistivity and 1.45° in phase and setting free the static shift distortion parameters during late-stage iterations so that they were automatically estimated by the code. Data consisted of 54 MT broadband sites (period range of 0.0008–1024 s), 25 of

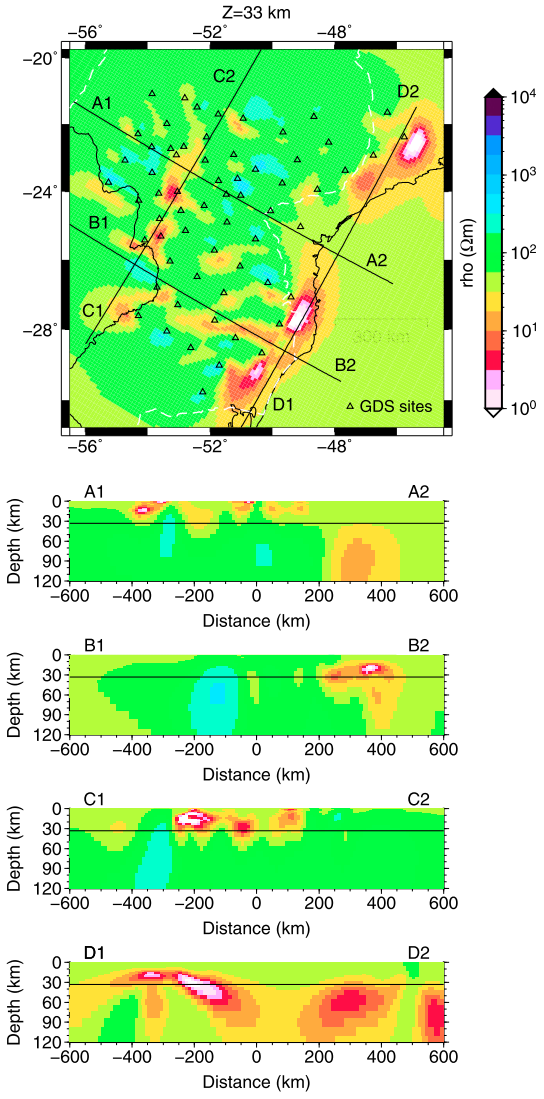

Figure 7. The preferred 3-D inversion model derived using a starting half-space resistivity of 50 Ω m. (top) A horizontal section of the geoelectrical model at a depth of 33 km, with the position of the GDS sites, Paraná Basin limits (dashed white lines), and the location of the four chosen profiles. (bottom) Panels showing vertical resistivity sections along the four vertical profiles, where the solid black line indicates the depth of the horizontal slice shown above.

which also included long-period data (10–13,653 s). The initial models were either uniform half-spaces or a layered half-space determined from 1-D inversion of the geometric mean of all sites, and all gave essentially the same final resistivity models (see Figure S4 in the supporting information). The preferred 2-D inversion model shown in Figure 6 was derived using a starting half-space resistivity of 100 Ω m and allowed acceptable misfits between observations and model predictions with an overall root-mean-square (RMS) of 1.66, related to the assumed error floors. A detailed comparison between the data and model responses for the whole data set can be found in the supporting information (Figure S5).

Figure 6 also shows the estimated static shift coefficients and RMS misfits at each of the stations. Both the RMS errors and the static shift coefficients show a general trend from lower values at sites over the Paraná Basin to higher values at sites over the Rio Apa block. The larger misfits in the western end of the profile is likely due to 3-D effects in the resistive rocks of the Rio Apa block not removed during distortion decomposition. On the other hand, the larger static shifts affected more the TM mode, with some of the apparent resistivity curves shifted upward by current deflection at soundings directly above surficial resistive bodies in the Rio Apa block. However, the scattering due to static shift was not significant, with corrections smaller than a logarithmic decade.

Resistive lithosphere (up to 10,000 Ω m) is observed beneath the Rio Apa block and the western side of the Paraná Basin. It is locally truncated by isolated conductors observed in the lower crust/upper mantle beneath the Cenozoic sedimentary package that covers the Rio Apa block on the western end of the profile and close to the edge of the basin. Occurrences of several alkaline-carbonatitic complexes mostly found along the rim of the basin support the possible presence of similar complexes hidden beneath the Paraná Basin. MT soundings over one of these outcropping carbonatitic complexes in the Alto Paranaíba igneous province, at the northeastern basin border, show signatures of enhanced conductivity at crustal depths related to the alkaline magmatism [*Bologna et al.,* 2011] very similar to those anomalies observed in our 2-D geoelectrical model of Figure 6. Consequently, some of these isolated conductors beneath the Paraná Basin can be associated with localized round pipe-shaped carbonatitic intrusions.

On the other hand, the basement under the central part of the Paraná Basin, around the Paraná River, and under the eastern portion of the profile presents low resistivity for an expected cold and dry lithosphere, with values between 300 and 1000 Ω m. The conductive anomaly mapped by the GDS data in Figure 5,

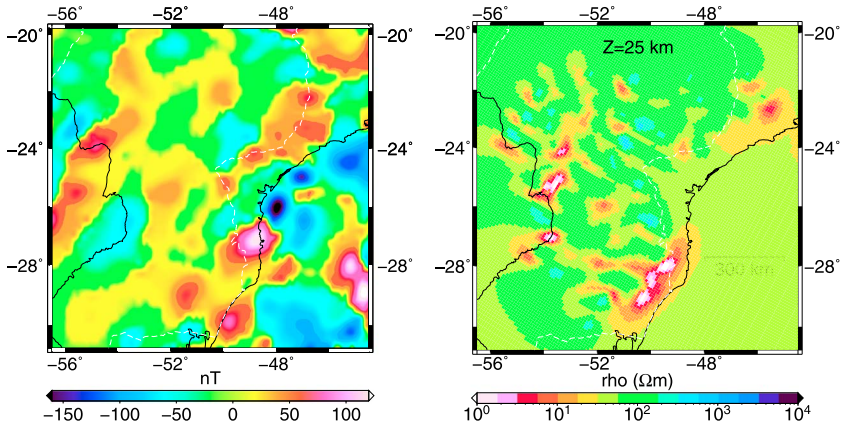

Figure 8. Comparison between the magnetic anomaly map (total component) for the Paraná Basin and surrounding region with a horizontal section of the geoelectrical model at a depth of 25 km. The magnetic map was derived from the NGDC-720 [*Maus*, 2010], with anomalies calculated at 1 km over sea level.

along the central part of the C1-C2 profile, is located east of the Paraná River, with lateral extent of less than 40 km and resistivity of less than 10 Ω m. This lateral extension is less than the one inferred from the 3-D inversion of the GDS data, but it should be noted that the spacing between the GDS soundings is around 100 km in this region and therefore cannot map in detail the horizontal location and width of the anomaly.

Regarding the constraints on the depth of this anomalous structure imaged by the 3-D GDS inversions, the top of the conductive anomaly in the 2-D model of Figure 6 is located in the upper crust near the bottom of the Paleozoic sedimentary package of the Paraná Basin. Among the three results shown in the C1-C2 traverse of Figure 5, the one that most closely matches this result in terms of depth of the anomalous body is the model derived with the inversion starting with a 50 Ω m half-space. Also, geoid anomalies located in the south São Francisco Craton [*Pinto et al.*, 2010] and in the Brazilian southern continental margin [*Leite*, 2000] that may have the same anomalous source as the deep geoelectric anomalies in these regions (see discussion in *Pinto et al.* [2010]) present good depth correlation with the model derived from the inversion of the 50 Ω m half-space. Consequently, the 50 Ω m half-space was the one chosen for subsequent analyzes.

4.3. Final 3-D Inversion Results

The final 3-D model, shown in Figure 7, is represented as a horizontal section at the depth of 33 km (Figure 7, top) and vertical slices down to 120 km depth along four chosen profiles (comparison between the data and model responses is presented in Figure S2 in the supporting information). These profiles are located in near coincidence with some of the main geologic features of the area and will be discussed in the next section. The most noteworthy features of the horizontal section are the sinuous, quasi-linear conductive zones underneath the sedimentary layers which strike approximately in the NNE direction mostly in the central Paraná Basin and in the WNW direction in the southern Paraná Basin. More widespread conductivity anomalies occur at the limits of the array coverage, beneath the extreme southeastern São Francisco Craton and Neoproterozoic fold belt (centered nearly at 45°W, 22°S) and along the southeastern border of the basin and in the continental margin (south of 27°S).

Figure 8 shows a magnetic crustal anomaly map for the Paraná Basin and its borders extracted from the third version of the National Geophysical Data Center's degree-720 integrated magnetic model [*Maus*, 2010]. The coefficients of this model were derived from the global Earth Magnetic Anomaly Grid (EMAG2), compiled from satellite (CHAMP) and available marine and aeromagnetic measurements [*Maus et al.*, 2009]. Unfortunately, there is a blank area in the EMAG2 grid compilation for an extensive region in the southern Paraná Basin, which limits the study of crustal characteristics of this area from the NGDC-720 model. For comparison, the figure also shows a horizontal section of the 3-D geoelectric model at the depth of 25 km. In spite of the limited resolution of the magnetic anomaly map to detect signatures of small spatial scales in this region, there is correlation between some of the linear conductive anomalies and major positive magnetic anomalies mapped in the basin and its borders. This is particularly true for the conductive anomalies along profiles B1-B2 and D1-D2, which are well correlated with strong magnetic anomalies.

Conductive anomalies detected along profile A1-A2 (Ponta Grossa Arch) are not correlated with magnetic anomalies due to the low resolution of this magnetic map but are well documented by more detailed aeromagnetic surveys [*Ferreira*, 1982]. The EM anomalies along profile C1-C2 lie at the eastern border of a remarkable positive NNE-SSW magnetic anomaly, roughly parallel to the main axis of the basin.

The bottom of the magnetized bodies is estimated by the Curie temperature at which crustal rocks lose their magnetism. Using a one-dimensional heat conductive transport model and available geothermal gradient and heat flow values for the central part of the Paraná Basin [*Hurter and Pollack*, 1996], the depth of the Curie isotherm is estimated to be between 30 and 37 km in the central Paraná Basin region where most of the linear conductive anomalies are observed. The depth chosen to represent the horizontal section in Figure 7 (33 km) is close to the mean of the above values. The vertical slices in Figure 7 show that this is the maximum depth for most of the conductive anomalies beneath the basin, whereas deeper anomalies are observed in regions at the borders or outside the basin.

Because of the diffusive nature of EM propagation, the VTF data have a far-flung effect and consequently will sense information from structures outside the array. The deep high-conductivity anomaly beneath the São Francisco Craton/Neoproterozoic fold belt is not an artifact of the inversion process but a physical image of a probable metasomatized upper mantle lithosphere previously mapped by other studies [*Figueiredo et al.,* 2008; *Pinto et al.,* 2010]. On the other hand, the location and geometry of the deep highly conductive anomalous structure at the southeastern continent-ocean boundary cannot be well defined by our data but its limits are nearly coincident with the offshore Pelotas Basin [*Stica et al.,* 2014]. Similar to the south São Francisco Craton/Neoproterozoic fold belt, strong geoid and magnetic anomalies are also observed in this coastal region which gives support to a similar interpretation confirming a deep high-conductivity anomaly in the area.

5. Discussions and Interpretation

To understand the origin of the conductivity anomalies observed in the 3-D geoelectrical model, it is necessary to know the physical mechanisms involved in electrical conductivity enhancements of the Earth's interior. As dry silicate rocks are highly resistive, enhanced conductivity in the continental lithosphere is often attributed to minute amounts of high conductors in interconnected grain-boundary arrangements, including fluids with high ionic content, conducting minerals such as sulfides, iron oxides, or graphite films, and partial melting [*Nover*, 2005]. Some of these factors can be confidently ruled out in the study area. Given their short residence times, it is unlikely that fluids could remain trapped at middle-to-lower crustal depths since the last tectonomagmatic event in the region (Late Cretaceous). Partial melts also do not seem to be an option for enhancing the conductivity because heat flow measurements in the central part of the Paraná Basin indicate values in the range of 40–50 m W/m^2 [*Hurter and Pollack*, 1996], which are restrained by temperatures that are below the mantle solidus, too low even for incipient melting.

Expected high resistivities that could be associated with stable and cold cratonic lithosphere blocks under the Paraná Basin are not observed in our models, neither in the 3-D GDS model nor in the 2-D MT model. The detected pervasive moderate lithosphere conductivity enhancement underneath the sedimentary layers could be related to rock property changes resulting from geodynamic events involved in the initial basin subsidence (in the Neoproterozoic or Ordovician) or to magmatic residues from the later Cretaceous magma differentiation at crustal depths, or deeper. In both cases, the crystalline lithosphere could be impregnated by conducting minerals leading to increased conductivity by electronic conduction provided by an interconnected network of conducting solid phases of iron- or sulfide-bearing minerals. Otherwise, an overall slightly enhanced bulk conductivity of the lithosphere could be attained by discreet amounts of widely scattered iron sulfides and iron oxide impurities at grain boundaries of rock minerals, as indicated by laboratory results conducted by *Watson et al.* [2010].

For the localized high-conductivity anomalies, the quasi-linear elongated geometry of the conductive zones with limited lateral extent and spatial correlation with some magnetic anomalies indicate that conductive mineralogies accumulated preferentially along shear planes are the most likely sources of conductivity enhancement. Metallic films of mineral assemblages composed by graphite and sulfides have often been indicated in the literature as the cause of strong crustal anomalies detected by electromagnetic soundings, such as in *Frost et al.* [1989] and *Ducea and Park* [2000], respectively. Graphite can be precipitated from hot

(>600°C) magmatic fluids and is commonly observed in volcanic terranes [*Luque et al.,* 1998], provided contingent oxygen fugacity was not too high for the stability of graphite. Sulfides could have been derived at somewhat higher fugacities from percolating volatiles during the emplacement of the Cretaceous volcanics [*Helffrich et al.,* 2011]. In Paraná Basin, however, the coincidence between magnetic anomalies and some of the quasi-linear conductive zones and the correlation between the maximum depth for most of the conductive anomalies and an estimated Curie depth gives a strong support for mineral conductors presenting also high magnetic susceptibility, such as iron oxides and iron sulfides, as the main source of the conductivity enhancement. In this case, precipitation mechanisms also produce highly conductive magnetite [*Kakudate et al.,* 1979] and other highly conducting accessory oxide phases, such as pyrrhotite [*Worm et al.,* 1993], when hot CO2-rich magmatic fluids under the proper fugacity conditions react with crustal iron-titanium-rich oxides [*Glover*, 1996].

5.1. A1-A2 Traverse: Ponta Grossa Arch

The Ponta Grossa Arch is a major tectonic structure located on the central eastern edge of the Paraná Basin and uplifted just prior to the voluminous continental flood basalt event that occurred in Early Cretaceous [*Strugale et al.,* 2007]. It is marked by a NW trending structure, characterized by ubiquitous megafault zones intruded by a large number of diabase dikes related to the tholeiitic magmatism of the Paraná Basin. In addition to the diabase dikes, there are several alkaline intrusions in the region, with chronological links with the tholeiitic effusives and associated dikes and sills of the main magmatic phase of the arch. The available aeromagnetic data indicate that dike swarms extend for at least 300 km under the basaltic cover toward the basin depocenter [*Ferreira*, 1982].

The A1-A2 traverse of Figure 7 is positioned in nearly coincidence with the trace of the arch and the MT profile across the central part of the basin. Unfortunately, the exclusion of the 38 easternmost MT sites due to noise and different strike direction does not allow a good comparison between the two geoelectric models of Figures 6 and 7. The conductive anomaly mapped by the C1-C2 profile and located transversely at the eastern side of the MT profile is also seen at the distance −200 km in the A1-A2 profile. Horizontal location and vertical extent of the anomalous structure are correctly mapped by the 3-D model, but the geometry and the absolute value of the anomalous resistivity are not properly resolved, which can be attributed to the large spacing between stations and the inherent limited resolution of the GDS data.

The upper-to-middle crust anomalies detected in the A1-A2 traverse in distances roughly between −100 and 200 km on the profile are probably related to the evolution of the Ponta Grossa Arch. Their location and horizontal extension coincide with the dike-swarm positions detected by the aeromagnetic data. These dikes were injected within a brief time interval subsequent to the main basaltic effusion in the basin [*Renne et al.,* 1996] during the thermal doming of the mantle. They are interpreted as part of the feeder-channel system of the Early Cretaceous continental flood basalts and might be genetically related to the synrift stage of the formation of the South Atlantic [*Zalán et al.,* 1990].

As previously discussed, the detected high-conductivity anomalies could be related to conductive mineralogies (graphite, sulfide, and iron oxides) smeared on the planes of sheared fault zones. The faults beneath the Ponta Grossa Arch were associated to the tectonic uplift of the area and used as lava conduits at the time of the basalt flows. From the maximum depth of the conductive anomalies these faults would be rooted down to a ductile middle-lower crust.

5.2. B1-B2 Traverse: Torres Syncline

The NW plunging Torres Syncline is a large folded structure in the south Brazilian margin that constitutes the southeasternmost outcrops of volcanic rocks of the Paraná Basin. It has been characterized mainly through the superficial observation of the set of faults that vertically moved the sedimentary layers of the basin but its importance in the evolutionary history of the basin is still unclear. To account for the short time interval within which the volcanic activity took place, it has been suggested that the lava flows outpoured simultaneously from conduits established contemporaneously at different parts of the Paraná Basin, one of them being the Torres-Posadas lineament, a WNW extension of the Torres Syncline [*Petri and Fúlfaro*, 1983]. On the contrary, *Hartmann et al.* [2013] reported that no significant dip of the lava flows toward the center of the syncline is observed, with faulting being the main geological process related to its evolution during the opening of the Atlantic Ocean.

A previous MT/GDS study carried out in the Torres Syncline (see locations of the stations in Figure 1) defined a shallow conductive anomaly with a NW trend, roughly coincident with the trace of the syncline. It was interpreted as a concentration of highly mineralized fluids in a vertically fractured zone related to the magmatic activity [*Padilha and Vitorello*, 2000].

The horizontal section of Figure 7 shows a WNW nearly linear conductive anomaly in the southern part of the basin, starting on the Torres Syncline at the continental coast and running westward toward the inland. Inward, the conductor changes its direction to E-W near the center of the basin, not following exactly the trace of the Torres-Posadas lineament. The vertical B1-B2 traverse is roughly aligned with the Torres-Posadas lineament and cuts the eastern side of this anomaly (distances between 200 and 400 km on the profile). It shows that the conductor is very deep in the SE corner at the profile distance of 400 km and its top dips northwest at shallow depths. Conductive mineralogies along shear planes are the most likely cause that would explain the deep enhanced conductivity beneath the Torres Syncline.

5.3. C1-C2 Traverse: Paraná River

The NNE elongated conductive anomaly seen in Figure 7 at the central part of the basin, roughly parallel to the present-day Paraná River, has already been surmised from the qualitative analysis of the induction arrows of Figure 4. The MT data (Figure 6) show the subvertical conductor at 70 km east of Paraná River and that it extends down throughout the crust with limited lateral extent. Its position and direction coincide with the depocenter [*Zalán et al.,* 1990], which has been taken as the probable location of the rifting that led to the initial subsidence of the basin [*Milani and Ramos*, 1998]. Also, this region parallel to the Paraná River has been proposed to be the major location axis from where the extrusion of lava flows first took place [*Janasi et al.,* 2011]. These observations are consistent with the presence of an old zone of mechanical weakness that had a strong influence on the initial Paleozoic subsidence of the basin and later favored the intraplate magmatism. A likely explanation for the high conductivity along the C1-C2 traverse is the occurrence of volatile percolation followed by precipitation of conductive minerals during the magmatic ascent along the old weakness zone.

5.4. D1-D2 Traverse: A Possible Relation With the Offshore Pelotas Basin?

Figure 7 shows a broad high-conductivity anomaly along the continent-ocean transition of the Brazilian southern margin. This area is beyond the array coverage, and consequently, the result should be treated with caution. Although the position and geometry of the structure cannot be inferred from the data because of the absence of marine coverage, its general trend and correlation with the magnetic anomaly probably reflects the presence of a strong conductivity anomaly along the coast. The northern limit of this anomaly is nearly coincident with the boundary between the offshore Pelotas and Santos Basins (Florianópolis fracture zone). Following *Stica et al.* [2014], this boundary also marks the passage of a system of volcanic basins in the southern segment (extending from Argentina to the Pelotas Basin) to a system of magma-poor basins in the northern segment (Santos, Campos, and Espírito Santo Basins).

The passive margin of South America originated with the onset of the rupture and final separation of West Gondwana during the Early Cretaceous. On the Pelotas Basin, thick wedges of reflectors dipping toward the ocean (seaward dipping reflectors) are interpreted as volcanic and volcaniclastic rocks deposited in a rift environment of a volcanic passive margin [*Stica et al.,* 2014]. Other geophysical data from the southern/southeastern part of the South American continental margin show linear anomalies accompanying the coast, interpreted as a marginal trough filled with volcanic rocks [*Rabinowitz and LaBrecque*, 1979; *Mio et al.,* 2005]. Also, residual geoid anomalies indicate positive values along the coast in the region where the conductivity anomaly is possibly located [*Leite*, 2000]. All these results point to a concentration of igneous intrusions in the zone of crustal rupture that could present high magnetization and high oxide and sulfide mineral content. Thus, we further speculate that the broad high-conductivity anomaly along the Brazilian southern continental margin can also be linked to the magmatic activity related to the continental breakup but probably already in the process of lithospheric extension.

6. Conclusions

Integration between GDS and MT data allowed the mapping of a well-defined structural pattern for the conductivity distribution of the lithosphere of southern Brazil. The continental crust presents several mainly

subvertical zones of enhanced conductivity, coincident with some of the main tectonic structures recognized at the surface and with magnetic anomalies, and a moderate overspread conductivity enhancement beneath the central part of the Paraná Basin, unexpected for a postulated cratonic basement, normally expected to be resistive. A broad high-conductivity anomaly is also observed along the continental margin, but this result has to be considered with caution because the region is outside the area of data coverage.

It is proposed that the subvertical quasi-linear high-conductivity anomalies are related to crustal shear zones that served as paleofluid pathways. They are closely related to some of the major tectonic structure across the basin and magnetic anomalies. Thus, these shear zones are likely associated both with deep and older (Precambrian) zones of mechanical weakness, posteriorly involved in the initial Paraná Basin subsidence and with the effects of local and younger (Early Cretaceous) thermal events that occurred just before the onset of the main volcanic activity. A cryptic NNE fault zone extending throughout the crust and hidden underneath the central part of the basin (parallel to the Paraná River) may represent a Late Precambrian mechanically weak zone that played a considerable role on the development of tectonic sedimentary structures of the basin and that later facilitated the basaltic flows. In the geoelectrical model, the NW faults along the Ponta Grossa Arch are shown to extend down to the midcrust and are examples of structures derived from a local tectonic uplift in the Early Cretaceous. The Torres Syncline is also presented as a deep-rooted shear zone, which deepens toward the center of the basin but does not follow the proposed trace of the Torres-Posadas lineament. This finding supports previous assumptions about the importance of this structure as a conduit for the outpouring of lava in the Early Cretaceous.

Localized conductivity anomalies in ancient provinces are commonly interpreted as retained imprints of fossil tectonic processes. In the Paraná Basin, upward movement of CO^2-bearing volatiles through discrete fault zones during the emplacement of basalts is the likely source of the enhanced conductivity seen by surface GDS and MT measurements. Even after the fluid propagation had ceased, the precipitated solid phase products left behind in shear zones would retain high conductivities. Correlation between magnetic anomalies and the conductivity structure gives strong support for the hypothesis that iron oxides and iron sulfides are the most likely source of the enhanced conductivity. Magnetite and pyrrhotite, in particular, can be very conductive at typical crustal depths, and its deposition along shear zones can provide electrical connection across large distances. However, other highly conducting mineral phases related to volatile percolation such as graphite cannot be discarded as a possible source.

Models so far proposed for the configuration of the crystalline basement beneath the basin include a central impaired cratonic nucleous or an amalgamation of independent sutured cratonic blocks. Both models would presume an underlying stable refractory lithosphere for the cratonic root that would not facilitate the upwelling of hot tholeiitic magma melts from a more fertile source. However, the middle to lower crust and the top of the lithospheric mantle under the central part of the basin show an increase in conductivity across a wide area, which is compatible with a more fertile or a much less refractory rock type dominating the shallower levels of the mantle. Our data show that the whole crust was affected by conducting minerals either related to the tectonic event in the Ordovician/Late Precambrian that led to the initial subsidence of the basin or to contamination by Cretaceous magmatic materials that would not be restricted to the top (Paraná Basin) and the base (magmatic underplating) of the crust. Because subsurface geoelectrical models can reflect different snapshots of various stages in lithosphere evolution over time, independent geophysical information will be necessary to discern between these possibilities.

Acknowledgments

The GDS and MT transfer functions used to derive the inversion models are available upon request to the corresponding author (antonio.padilha@inpe.br). This study was supported by research grants and fellowships from FAPESP (03/10817-2, 09/50493-8, and 09/13054-6) and CNPq (302347/08-9 and 303813/09-1). The authors are grateful to François Chamalaun, for loaning the fluxgate magnetometers of Flinders University for the GDS array, Gary Egbert, for providing the software packages for data processing and 2-D and 3-D inversions, Naomi Ussami, for discussions and preparing the data used in Figure 8, and the dedicated field and lab crew of the geomagnetism group at INPE. We thank two anonymous reviewers and the Associate Editor for their comments that helped to improve the manuscript.

References

Abdu, M. A., I. S. Batista, A. J. Carrasco, and C. G. M. Brum (2005), South Atlantic magnetic anomaly ionization: A review and a new focus on electrodynamic effects in the equatorial ionosphere, *J. Atmos. Sol. Terr. Phys.*, *67*, 1643–1657, doi:10.1016/j.jastp.2005.01.014.

Allen, P. A., and J. J. Armitage (2012), Cratonic basins, in *Tectonics of Sedimentary Basins: Recent Advances*, edited by C. Busby and A. Azor, pp. 602–620, John Wiley, Ltd, Chichester, U. K., doi:10.1002/9781444347166.ch30

Antunes, C. E. (2012), Tomografia de condutividade elétrica sob a bacia do Paraná utilizando dados do campo geomagnético, MS thesis, INPE, São José dos Campos, Brazil.

Arora, B. R., A. Rigoti, Í. Vitorello, A. L. Padilha, N. B. Trivedi, and F. H. Chamalaun (1998), Magnetometer array study in north-northeast Brazil: Conductivity image building and functional induction modes, *Pure Appl. Geophys.*, *152*, 349–375, doi:10.1007/s000240050158.

Arora, B. R., A. L. Padilha, Í. Vitorello, N. B. Trivedi, S. L. Fontes, A. Rigoti, and F. H. Chamalaun (1999), 2-D geoelectrical model for the Parnaíba Basin conductivity anomaly of northeast Brazil and tectonic implications, *Tectonophysics*, *302*, 57–69, doi:10.1016/S0040-1951(98)00272-8.

Assumpção, M., M. Bianchi, J. Julià, F. L. Dias, G. S. França, R. Nascimento, S. Drouet, C. G. Pavão, D. F. Albuquerque, and A. E. V. Lopes (2013), Crustal thickness map of Brazil: Data compilation and main features, *J. South Am. Earth Sci.*, *43*, 74–85, doi:10.1016/j.jsames.2012.12.009.

Bellieni, G., P. Comin-Chiaramonti, L. S. Marques, A. J. Melfi, E. M. Piccirillo, A. J. R. Nardy, and A. Roisenberg (1984), High- and low-TiO_2 flood basalts from the Paraná Plateau (Brazil): Petrology and geochemical aspects bearing on their mantle origin, *Neues Jahrb. Mineral Abh.*, *150*, 273–306.

Bizzi, L. A., C. Schobbenhaus, J. H. Gonçalves, F. J. Baars, I. M. Delgado, M. B. Abram, R. Leão Neto, G. M. M. Matos, and J. O. S. Santos (2001), *Geologia, Tectônica e Recursos Minerais do Brasil: Sistema de Informações Geográficas–SIG e Mapas na Escala 1:2,500,000*, Companhia de Pesquisa de Recursos Minerais, Brasília, Brazil.

Bologna, M. S., A. L. Padilha, Í. Vitorello, and M. B. Pádua (2011), Signatures of continental collisions and magmatic activity in central Brazil as indicated by a magnetotelluric profile across distinct tectonic provinces, *Precambrian Res.*, *185*, 55–64, doi:10.1016/j.precamres.2010.12.003.

Bologna, M. S., A. L. Padilha, M. B. Pádua, Í. Vitorello, and F. H. Chamalaun (2014), Paraguay-Araguaia belt conductivity anomaly: A fundamental tectonic boundary in South American Platform imaged by electromagnetic induction surveys, *Geochem. Geophys. Geosyst.*, *15*, 509–515, doi:10.1002/2013GC004970.

Chamalaun, F. H., and R. Walker (1982), A microprocessor based digital fluxgate magnetometer for geomagnetic deep sounding studies, *J. Geomagn. Geoelectr.*, *34*, 491–507.

Cordani, U. G., B. B. Brito-Neves, R. A. Fuck, R. Porto, A. Tomaz Filho, and F. M. B. Cunha (1984), Estudo preliminar de integração do Pré-Cambriano com os eventos tectônicos das bacias sedimentares Brasileiras, PETROBRÁS/CENPES/SINTEP Rep. 15, 70 pp., Rio de Janeiro, Brazil.

Ducea, M. N., and S. K. Park (2000), Enhanced mantle conductivity from sulfide minerals, southern Sierra Nevada, California, *Geophys. Res. Lett.*, *27*, 2405–2408, doi:10.1029/2000GL011565.

Egbert, G. D. (1997), Robust multiple-station magnetotelluric data processing, *Geophys. J. Int.*, *130*, 475–496.

Egbert, G. D. (2002), Processing and interpretation of electromagnetic induction array data, *Surv. Geophys.*, *23*, 207–249.

Egbert, G. D., and J. R. Booker (1989), Multivariate analysis of geomagnetic array data: 1. The response space, *J. Geophys. Res.*, *94*, 14,227–14,247, doi:10.1029/JB094iB10p14227.

Egbert, G. D., and A. Kelbert (2012), Computational recipes for electromagnetic inverse problems, *Geophys. J. Int.*, *189*, 251–267, doi:10.1111/j.1365-246X.2011.05347.x.

Ernesto, M., L. S. Marques, E. M. Piccirillo, E. C. Molina, N. Ussami, P. Comin-Chiaramonti, and G. Bellieni (2002), Paraná Magmatic Province-Tristan da Cunha plume system: Fixed versus mobile plume, petrogenetic considerations and alternative heat sources, *J. Volcanol. Geotherm. Res.*, *118*, 15–36, doi:10.1016/S0377-0273(02)00248-2.

Evans, R. L. (2012), Conductivity of Earth materials, in *The Magnetotelluric Method: Theory and Practice*, edited by A. D. Chave and A. G. Jones, chap. 3A, pp. 50–95, Cambridge Univ. Press, New York.

Ferreira, F. J. F. (1982), Alinhamentos estruturais-magnéticos da região centro-oriental da Bacia do Paraná e seu significado tectônico, in *Bacia do Paraná - Reavaliação da Potencialidade e Prospectividade em Hidrocarbonetos*, Rep. 12, pp. 143–166, CESP-IPT, São Paulo, Brazil.

Figueiredo, I., M. A. Meju, and S. L. Fontes (2008), Heterogeneous crust and upper mantle across the SE Brazilian Highlands and the relationship to surface deformation as inferred from magnetotelluric imaging, *J. Geophys. Res.*, *113*, B03404, doi:10.1029/2007JB005108.

Fraser-Smith, A. C. (1987), Centered and eccentric geomagnetic dipoles and their poles, 1600–1985, *Rev. Geophys.*, *25*, 1–16, doi:10.1029/RG025i001p00001.

Frost, B. R., W. S. Fyfe, K. Tazaki, and T. Chan (1989), Grain boundary graphite in rocks and implications for high electrical conductivity in the lower crust, *Nature*, *340*, 134–136, doi:10.1038/340134a0.

Fúlfaro, V. J., A. R. Saad, M. V. Santos, and R. B. Vianna (1982), Compartimentação e evolução tectônica da Bacia do Paraná, *Rev. Bras. Geociênc.*, *12*, 590–611.

Gibson, S. A., R. N. Thompson, O. H. Leonardos, A. P. Dickin, and J. G. Mitchell (1995), The Late Cretaceous impact of the Trindade mantle plume: Evidence from large volume, mafic, potassic magmatism in SE Brazil, *J. Petrol.*, *36*, 189–229.

Glover, P. W. J. (1996), Graphite and electrical conductivity in the lower continental crust: A review, *Phys. Chem. Earth*, *21*, 279–287, doi:10.1016/S0079-1946(97)00049-9.

Gomes, C. B., and P. Comin-Chiaramonti (2005), An introduction to the alkaline and alkaline-carbonatitic magmatism in and around the Paraná Basin, in *Mesozoic to Cenozoic Alkaline Magmatism in the Brazilian Platform*, edited by P. Comin-Chiaramonti and C. B. Gomes, pp. 21–29, EDUSP/FAPESP, São Paulo, Brazil.

Groom, R. W., and R. C. Bailey (1989), Decomposition of magnetotelluric impedance tensors in the presence of local three-dimensional galvanic distortion, *J. Geophys. Res.*, *94*, 1913–1925, doi:10.1029/JB094iB02p01913.

Hartmann, L. A., K. R. Arena, S. K. Duarte, and J. Pertille (2013), Long-distance lava correlation in the Paraná volcanic province along the Serra Geral cuesta, southeastern Brazil, *Int. J. Earth Sci.*, *102*, 1655–1669, doi:10.1007/s00531-013-0899-z.

Helffrich, G., J.-M. Kendall, J. O. S. Hammond, and M. R. Carroll (2011), Sulfide melts and long-term low seismic wavespeeds in lithospheric and asthenospheric mantle, *Geophys. Res. Lett.*, *38*, L11301, doi:10.1029/2011GL047126.

Hulot, G., C. Eymin, B. Langlais, M. Mandea, and N. Olsen (2002), Small-scale structure of the geodynamo inferred from Oersted and Magsat satellite data, *Nature*, *416*, 620–623, doi:10.1038/416620a.

Hurter, S. J., and H. N. Pollack (1996), Terrestrial heat flow in the Paraná Basin, southern Brazil, *J. Geophys. Res.*, *101*, 8659–8671, doi:10.1029/95JB03743.

Janasi, V. A., V. A. de Freitas, and L. H. Heaman (2011), The onset of flood basalt volcanism, Northern Paraná Basin, Brazil: A precise U-Pb baddeleyite/zircon age for a Chapecó-type dacite, *Earth Planet. Sci. Lett.*, *302*, 147–153, doi:10.1016/j.epsl.2010.12.005.

Julià, J., M. Assumpção, and M. P. Rocha (2008), Deep crustal structure of the Paraná Basin from receiver functions and Rayleigh-wave dispersion: Evidence for a fragmented cratonic root, *J. Geophys. Res.*, *113*, B08318, doi:10.1029/2007JB005374.

Kakudate, Y., N. Mori, and Y. Kino (1979), Pressure effect on the anomalous electrical conductivity of magnetite, *J. Magn. Magn. Mater.*, *12*, 22–25, doi:10.1016/0304-8853(79)90329-9.

Klein, G. V., and A. T. Hsui (1987), Origin of cratonic basins, *Geology*, *15*, 1094–1098, doi:10.1130/0091-7613(1987)15<1094:OOCB>2.0.CO;2.

Leite, E. P. (2000), Interpretação de anomalias do geóide e ar-livre da margem continental sul do Brasil: Escudo Rio-Grandense e SE do Cone do Rio Grande, MS thesis, Universidade de São Paulo, São Paulo, Brazil.

Luque, F. J., J. D. Pasteris, B. Wopenka, M. Rodas, and J. F. Barrenechea (1998), Natural fluid-deposited graphite: Mineralogical characteristics and mechanisms of formation, *Am. J. Sci.*, *298*, 471–498.

Mantovani, M. S. M., M. C. L. Quintas, W. Shukowsky, and B. B. B. Neves (2005), Delimitation of the Paranapanema Proterozoic block: A geophysical contribution, *Episodes*, *28*, 18–22.

Mariani, P., C. Braitenberg, and N. Ussami (2013), Explaining the thick crust in Paraná Basin, Brazil, with satellite GOCE gravity observations, *J. South Am. Earth Sci.*, *45*, 209–223, doi:10.1016/j.jsames.2013.03.008.

Marques, A., O. A. Zanotto, A. B. França, M. A. M. Astolfi, and O. B. Paula (1993), Compartimentação tectônica da Bacia do Paraná, PETROBRAS/NEXPAR Report, 87 pp., Curitiba, Brazil.

Maus, S. (2010), An ellipsoidal harmonic representation of Earth's lithospheric magnetic field to degree and order 720, *Geochem. Geophys. Geosyst.*, *11*, Q06015, doi:10.1029/2010GC003026.

Maus, S., et al. (2009), EMAG2: A 2–arc min resolution Earth Magnetic Anomaly Grid compiled from satellite, airborne, and marine magnetic measurements, *Geochem. Geophys. Geosyst.*, *10*, Q08005, doi:10.1029/2009GC002471.

McNeice, G. W., and A. G. Jones (2001), Multisite, multifrequency tensor decomposition of magnetotelluric data, *Geophysics*, *66*, 158–173, doi:10.1190/1.1444891.

Melfi, A. J., E. M. Piccirillo, and A. J. R. Nardy (1988), Geological and magmatic aspects of the Paraná Basin: An introduction, in *The Mesozoic Flood Volcanism From the Paraná Basin (Brazil): Petrogenetic and Geophysical Aspects*, edited by E. M. Piccirillo and A. J. Melfi, pp. 1–13, IAG/USP, São Paulo, Brazil.

Milani, E. J., and V. A. Ramos (1998), Orogenias paleozóicas no domínio sul-ocidental do Gondwana e os ciclos de subsidência da Bacia do Paraná, *Rev. Bras. Geociênc.*, *28*, 473–484.

Mio, E., H. K. Chang, and F. S. Correa (2005), Integração de métodos geofísicos na modelagem crustal da Bacia de Santos, *Rev. Bras. Geof.*, *23*, 275–284.

Molina, E. C., and N. Ussami (1999), The geoid in southeastern Brazil and adjacent regions: New constraints on density distribution and thermal state of the lithosphere, *J. Geodyn.*, *28*, 357–374, doi:10.1016/S0264-3707(99)00015-0.

Molina, E. C., N. Ussami, N. C. de Sá, D. Blitzkow, and O. F. Miranda Filho (1988), Deep crustal structure under the Paraná Basin (Brazil) from gravity study, in *The Mesozoic Flood Volcanics of the Paraná Basin: Petrogenic and Geophysical Aspects*, edited by E. M. Piccirillo and A. J. Melfi, pp. 271–283, IAG/USP, São Paulo, Brazil.

Nover, G. (2005), Electrical properties of crustal and mantle rocks—A review of laboratory measurements and their explanation, *Surv. Geophys.*, *26*, 593–651, doi:10.1007/s10712-005-1759-6.

Padilha, A. L., and Í. Vitorello (2000), Magnetotelluric and geomagnetic depth soundings around the Torres Syncline hinge, Southeast Paraná Basin, Brazil, *Geophys. Res. Lett.*, *27*, 3655–3658, doi:10.1029/2000GL011507.

Padilha, A. L., N. B. Trivedi, Í. Vitorello, and J. M. da Costa (1992), Upper crustal structure of the northeast Paraná Basin, Brazil, determined from integrated magnetotelluric and gravity measurements, *J. Geophys. Res.*, *97*, 3351–3365, doi:10.1029/91JB02712.

Padilha, A. L., Í. Vitorello, and M. B. Pádua (2013), Deep conductivity structure beneath the northern Brasília belt, central Brazil: Evidence for a Neoproterozoic arc-continent collision, *Gondwana Res.*, *23*, 748–758, doi:10.1016/j.gr.2012.05.016.

Parkinson, W. D. (1959), Direction of rapid geomagnetic fluctuations, *Geophys. J. R. Astron. Soc.*, *2*, 1–14, doi:10.1111/j.1365-246X.1959.tb05776.x.

Parkinson, W. D., and F. W. Jones (1979), The geomagnetic coast effect, *Rev. Geophys.*, *17*, 1999–2015, doi:10.1029/RG017i008p01999.

Paulikas, G. A. (1975), Precipitation of particles at low and middle latitudes, *Rev. Geophys. Space Phys.*, *13*, 709–734.

Petri, S., and V. J. Fúlfaro (1983), *Geologia do Brasil: Fanerozóico*, 631 pp., TA Queiroz/Universidade de São Paulo, São Paulo, Brazil.

Pinto, L. G. R., M. B. Pádua, N. Ussami, I. Vitorello, A. L. Padilha, and C. Braitenberg (2010), Magnetotelluric deep soundings, gravity and geoid in the south São Francisco craton: Geophysical indicators of cratonic lithosphere rejuvenation and crustal underplating, *Earth Planet. Sci. Lett.*, *297*, 423–434, doi:10.1016/j.epsl.2010.06.044.

Rabinowitz, P. D., and J. LaBrecque (1979), The Mesozoic South Atlantic Ocean and evolution of its continental margins, *J. Geophys. Res.*, *84*, 5973–6002, doi:10.1029/JB084iB11p05973.

Renne, P. R., K. Deckart, M. Ernesto, G. Féraud, and E. M. Piccirillo (1996), Age of the Ponta Grossa dike swarm (Brazil), and implications to Paraná flood volcanism, *Earth Planet. Sci. Lett.*, *144*, 199–211, doi:10.1016/0012-821X(96)00155-0.

Rigoti, A., F. H. Chamalaun, N. B. Trivedi, and A. L. Padilha (1999), Characteristics of the equatorial electrojet determined from an array of magnetometers in N-NE Brazil, *Earth Planets Space*, *51*, 115–128, doi:10.1186/BF03352216.

Rocha, M. P., M. Schimmel, and M. Assumpção (2011), Upper-mantle seismic structure beneath SE and Central Brazil from P- and S-wave regional traveltime tomography, *Geophys. J. Int.*, *184*, 268–286, doi:10.1111/j.1365-246X.2010.04831.x.

Rocha-Júnior, E. R. V., I. S. Puchtel, L. S. Marques, R. J. Walker, F. B. Machado, A. J. R. Nardy, M. Babinski, and A. M. G. Figueiredo (2012), Re–Os isotope and highly siderophile element systematics of the Paraná continental flood basalts (Brazil), *Earth Planet. Sci. Lett.*, *337–338*, 164–173, doi:10.1016/j.epsl.2012.04.050.

Selway, K. (2014), On the causes of electrical conductivity anomalies in tectonically stable lithosphere, *Surv. Geophys.*, *35*, 219–257, doi:10.1007/s10712-013-9235-1.

Shimizu, H., A. Yoneda, K. Baba, H. Utada, and N. Palshin (2011), Sq effect on the electromagnetic response functions in the period range between 10^4 and 10^5 s, *Geophys. J. Int.*, *186*, 193–206, doi:10.1111/j.1365-246X.2011.05036.x.

Siripunvaraporn, W., and G. Egbert (2000), An efficient data-subspace inversion method for 2-D magnetotelluric data, *Geophysics*, *65*, 791–803, doi:10.1190/1.1444778.

Siripunvaraporn, W., and G. Egbert (2009), WSINV3DMT: Vertical magnetic field transfer function inversion and parallel implementation, *Phys. Earth Planet. Inter.*, *173*, 317–329, doi:10.1016/j.pepi.2009.01.013.

Soyer, W., and H. Brasse (2001), A magneto-variation array study in the central Andes of N Chile and SW Bolivia, *Geophys. Res. Lett.*, *28*, 3023–3026, doi:10.1029/2000GL012095.

Stanley, W. D., A. R. Saad, and W. Ohofugi (1985), Regional magnetotelluric surveys in hydrocarbon exploration, Paraná Basin, Brazil, *AAPG Bull.*, *69*, 346–360.

Stica, J. M., P. V. Zalán, and A. L. Ferrari (2014), The evolution of rifting on the volcanic margin of the Pelotas Basin and the contextualization of the Paraná-Etendeka LIP in the separation of Gondwana in the South Atlantic, *Mar. Pet. Geol.*, *50*, 1–21, doi:10.1016/j.marpetgeo.2013.10.015.

Strugale, M., S. P. Rostirolla, F. Mancini, C. V. Portela-Filho, F. J. F. Ferreira, and R. C. Freitas (2007), Structural framework and Mesozoic–Cenozoic evolution of Ponta Grossa Arch, Paraná Basin, southern Brazil, *J. South Am. Earth Sci.*, *24*, 203–227, doi:10.1016/j.jsames.2007.05.003.

Watson, H. C., J. J. Roberts, and J. A. Tyburczy (2010), Effect of conductive impurities on electrical conductivity in polycrystalline olivine, *Geophys. Res. Lett.*, *37*, L02302, doi:10.1029/2009GL041566.

Worm, H.-U., D. Clark, and M. J. Dekkers (1993), Magnetic susceptibility of pyrrhotite: Grain size, field and frequency dependence, *Geophys. J. Int.*, *114*, 127–137, doi:10.1111/j.1365-246X.1993.tb01472.x.

Zalán, P. V., S. Wolff, M. A. M. Astolfi, I. S. Vieira, J. C. J. Conceição, V. T. Appi, E. V. S. Neto, J. R. Cerqueira, and A. Marques (1990), The Paraná Basin, Brazil, in *Interior Cratonic Basins*, Mem. 51, edited by M. W. Leighton et al., pp. 681–708, AAPG, Tulsa, Okla.